6G BRAINS Deliverable D3.1

3D Laser measurement of one factory at Bosch with 3D cloud scanner and 3D hand scanner

Editor:	Diego Dupleich (FhG)
Deliverable nature:	Report (R)
Dissemination level: (Confidentiality)	Public (PU)
Contractual delivery date:	30 September 2021
Actual delivery date:	30 September 2021
Suggested readers:	Consortium members, reviewers, researchers
Version:	1.0
Total number of pages:	41
Keywords:	Point cloud, raytracing, propagation measurements, channel modelling, Industry 4.0

Abstract

The present report introduces the results of an extensive 3D laser measurement campaign with the objective of obtaining a precise raytracing model from point cloud data in an industrial environment. The measurements were conducted in a Bosch factory in Germany. The resulting model is tested with different raytracing tools and contrasted with multiband radio frequency measurements, simultaneously conducted in the same scenario. This raytracing model allows simulations with spatial consistency over the different bands of interest in 6G BRAINS, providing an accurate geometrical representation of the environment from the propagation properties for precise localization applications.

Disclaimer

The research leading to these results has received funding from the European Union Horizon 2020 Programme under grant agreement number 101017226 – *6G BRAINS – H2020-ICT-2020-2.*

Impressum

[Full project title]	Bring Reinforcement-learning Into Radio Light Network for Massive Connections
[Short project title]	6G BRAINS
[Number and title of work-package]	WP3: 6G Physical Propagation Measurements and Modelling, from Microwave to THz and OWC
[Number and title of task]	T3.1: Multi-Band (MW + mmWave + THz + OWC) Channel Measurements in the Industrial Network Environments and Industrial Applications T3.2: Analysis of measurement data and elaboration of the differences in wave propagation T3.3: Common fused channel model for the industrial network environments and industrial
[Document title]	3D Laser measurement of one factory at Bosch with 3D cloud scanner and 3D hand scanner
[Editor: Name, company]	Diego Dupleich, FhG
[Work-package leader: Name, company]	Diego Dupleich, FhG
[Estimation of PM spent on the Deliverable]	20 PMs

Executive summary

6G BRAINS envisions the integration of novel spectrum bands to support the development of ubiquitous smart wireless communications in industrial scenarios. Future industrial tasks and services rely on the simultaneous utilization of sub-6 GHz, mm-waves, THz, and optical wireless communications (OWC). The free blocks of spectrum available at THz and OWC enables the implementation of innovatively high data rate wireless links with enhanced capacity, reliability, and latency. Furthermore, THz and OWC allow resolution on 3D simultaneous localization and mapping (SLAM) of up to 1 mm accuracy. Therefore, reliable channel models based on empirical evidence addressing these frequencies are of exceptional importance for the design, performance evaluation, standardization, and deployment of the future 6G networks.

However, the development and parametrization of a single model covering such a wide spectrum of frequency bands and applications is challenging in multiple aspects. Localization and imaging applications require a precise correspondence between the geometrical properties of the propagated paths and the location of users and scatterers. Moreover, testing heterogeneous localization methods, based on the combination of localization methods in different bands, requires spatial consistency of the model not only in the spatial domain, but also in the frequency domain: the scatterers must be in the same position for the different simulated bands. While the 3GPP 38.901 spatial model covers from 0.5 GHz to 100 GHz, the stochastic approach on the modelling of scatterers limits the usability of these models in these scenarios. Therefore, models with deterministic component are more appropriate for these applications.

Depending on the parametrization and diversity of the constructive materials in the map, raytracing (RT) tools allow simultaneous simulations at different frequencies with a precise geometrical representation of the environment in the propagation parameters of the paths. Nonetheless, the comparability of the results with reality depends on the complexity of the RT map/model. Thus, obtaining an accurate RT model with a high level of details and large number of objects is of crucial importance.

Therefore, the goal in 6G BRAINS is to obtain a precise RT model from point cloud data from extensive 3D laser scans in an arbitrary industrial scenario. This model is preliminary validated with sub-6 GHz and mm-waves measurements. Later, it will be contrasted and calibrated with simultaneous sub-6 GHz, mm-waves, THz, and OWC measurements. Finally, the RT model will be extended with stochastic components considering different features identified in the analysis of measurements.

List of authors

Company	Author	Contribution
Fraunhofer IIS	Diego Dupleich	
Fraunhofer IIS	Niu Han	
UBRUNEL	John Cosmas	Section 2.4
UBRUNEL	Geoffrey Eappen	Section 2.4
UBRUNEL	Kareem Ali	Section 2.4

Table of Content

Executive summary 4
List of authors 5
Table of Content 6
List of figures and tables 7
Abbreviations 8
1 Introduction 10
1.1 Objective of this document 11
1.2 Relation to other deliverables within the WP3 12
1.3 Structure of this document 13
2 Overview of Ray Tracing as Channel Modelling Tool for Industry Scenarios 13
2.1 Key parameters in RT simulations 15
2.2 Channel impulse response from RT simulations 15
2.2.1 Inclusion of antenna patterns in the channel impulse response 16
2.2.2 Inclusion of bandwidth in the channel impulse response 16
2.3 Fused channel model: concept 17
2.4 Applications of Digital Twin 18
2.4.1 Radio Beam Control 18
2.4.2 RAN Scheduler 21
3 Methodology 21
3.1 Point cloud from 3D laser scans 22
3.2 CAD model from point cloud data 23
3.3 RT model 24
3.4 Channel simulations 25
4 Measurements, Analysis, and Results 25
4.1 RT model from point cloud data 25
4.2 Evaluation of different RT tools 30
4.3 Preliminary RT and RF measurements comparison 32
4.3.1 Measurement and simulation set-up 32
4.3.2 Geometry validation from PDPs 34
4.3.3 Geometry validation from PAEPs 36
5 Summary and Concluding Remarks 37
References 39

List of figures and tables

Figure 1 – Workflow from 3D laser scans to RT simulations 11
Figure 2 - Relation between workflow and deliverables 12
Figure 3 - Simulated CIR with infinite and limited bandwidth (a) complete, and (b) detail. 17
Figure 4 - Concept of the fused channel model 18
Figure 5 - Radio beam control 19
Figure 6 - Hardware and software tools used during the different processing steps 21
Figure 7 - Pictures of the laser scanners used during the measurements: (a) Leica BLK360, and (b) Artec Leo. .. 22
Figure 8 - Positions of the BLK360 laser scanner during the measurements process 23
Figure 9 - Magnetic tag with reference pattern for hand-held scanner 23
Figure 10 – Modelled portion within the complete map of the factory hall 25
Figure 11 - Point cloud obtained from laser scans in the selected scenario 26
Figure 12 - (a) Point cloud and (b) CAD model of the measured portion of the scenario (without ceiling for visualization purposes) 26
Figure 13 – Pictures and CAD model of the different parts of the scenario 27
Figure 14 - (a) Machine scanned with the hand-held scanner, and (b) CAD model 28
Figure 15 - (a) CAD model and (b) RT model in Winprop (without ceiling) 29
Figure 16 - Example of the visualization of a simulation with the industry model using (a) MATLAB raytrace toolbox and (b) WinProp 30
Figure 17 – Example of a PDP using the same model but different RT tools 31
Figure 18 - (a) Ray visible with MATLAB raytrace tool and (b) not visible in the WinProp tool 31
Figure 19 - Composite picture taken by the channel sounder at the TX and the different measurement lines (L1 to L4) 33
Figure 20 - Picture of the scenario and RT simulation with the position of the TX used during the RF measurements 34
Figure 21 – Geometrical properties of the scenario from the PDPs at 60 GHz over different positions (a) from RT simulations with finite bandwidth, and (b) from measured PDPs 35
Figure 22 - Interpretation of the scatterers from RT simulations 36
Figure 23 - Measured power azimuth/elevation profile and RT simulation for a single position in track L1 at (a) 6.75 GHz, (b) 30 GHz, and (c) 60 GHz 37

Table 1 - Key parameters of RT tools 15
Table 2 - Initial electromagnetic properties of materials 24
Table 3 - RT simulations parameters 33

Abbreviations

3GPP	3rd Generation Partnership Project
5G	Fifth Generation (mobile/cellular networks)
5G PPP	5G Infrastructure Public Private Partnership
6G BRAINS	Bringing Reinforcement learning Into Radio Light Network for Massive Connections
AMC	Adaptive Modulation and Coding
AP	Access Point
ASA	Azimuth Spread of Arrival
ASD	Azimuth Spread of Departure
BS	Base Station
CAD	Computer-aided Design
CQI	Channel Quality Index
DMC	Dense Multipath Component
DNN	Deep Neural Network
DoA	Direction of Arrival
DoD	Direction of Departure
DRL-NN	Deep Reinforcement Learning – Neural Network
GO	Geometrical Optics
GTD	Geometrical Theory of Diffraction
GTP	Geometrical Theory of Propagation
IAB	Integrated Access and Backhaul
ISAC	Integrated Sensing and Communication
IoT	Internet of Things
KPI	Key Performance Indicator
LSP	Large Scale Parameter

M2M	Machine to Machine
MCS	Modulation and Coding Scheme
MLBS	Maximum Length Binary Sequence
MPC	Multi-Path Component
NN	Neural Network
PDP	Power Delay Profile
RT	Raytracing
RX	Receiver
SCM	Spatial Channel Model
SISO	Single Input Single Output
SLAM	Simultaneous Localization and Mapping
ToF	Time of Flight
UE	User Equipment
SCM	Spatial Channel Model
SINR	Signal-to-Interference-Plus-Noise Ratio
SNR	Signal-to-Noise Ratio
TX	Transmitter
WP3	Work Package Three

1 Introduction

Channel models are key enablers for the design and development of communication systems, allowing the prediction of the channel in different situations for testing the response of systems and algorithms.

The main challenge within the applications foreseen in 6G BRAINS is to obtain a single channel model with the capabilities to cover all the testing requirements:

- Multiband simulations: base stations (BS) and user equipment (UE) might operate simultaneously with multiple radio interfaces at different frequencies. Therefore, the model must provide a frequency dependent channel impulse response (CIR).
- Correlation over the different bands given by the geometrical properties of the location of the scatterers: this enables simulations to test inter-band algorithms, as assisted beamforming, or heterogeneous multiband localization methods, in which certain properties related to the position of the user can be estimated at lower frequencies, and then, the large available bandwidths at higher frequencies can be used to increase the accuracy.
- Realistic in terms of the geometrical description of the environment from the delay and angular propagation properties. Applications as imaging and localization rely on the geometrical properties of the scattered paths.

The complexity of the models depends on the properties of the systems and the parameters under test. For example, if a SISO system is under test and the evaluation parameter is coverage or received signal-to-noise ratio (SNR), empirical path-loss models offer an efficient trade-off between complexity and accuracy. On the other hand, at high frequencies, high gain or multi-antenna systems usually employ hybrid beamformers in which the analog component steers the array gain in the direction of the dominant paths to compensate the isotropical path-loss. Therefore, the geometrical properties of the environment, and propagation parameters as time of flight (ToF), direction of arrival (DoA), and direction of departure (DoD) become fundamental in these models, and we usually refer to them as spatial channel models (SCMs), since the spatial information of the channel is considered within the simulated parameters.

In addition, aspects as spatial consistency become more relevant when mobile systems under test requires the knowledge of the location of the scatterers during displacement, as they need to consistently track the location of the source of scattered signal for pointing the gain of the antennas. Also, applications as localization need an accurate description of the simulated environment to test realistic conditions.

Models are frequently classified into deterministic or stochastic. The former ones are characterized by offering the same channel realization in every run, and the latter generates different realizations of the channel in every execution, since the output is based on statistical distributions. A third type of classification that is currently gaining relevance for channel models in high frequency applications are the hybrid models. These models combine deterministic and stochastic components to address different features of the channel [1], [2]. Usually, the deterministic part is based on simplified RT calculations, and the stochastic is derived from statistics obtained from extensive measurement campaigns.

RT is a deterministic methodology for propagation modelling based on the geometrical theory of propagation (GTP). GTP is an extension of geometrical optics (GO) including geometrical

theory of diffraction (GTD). GTP is based on the concepts of rays to treat the different propagation mechanisms: reflection and transmission on plane surfaces and diffraction on edges. The main assumptions in RT are far-field (electromagnetic waves are considered as plane waves) and high frequency (the wavelength is small compared to the objects in the environment). In addition, different methods can also be incorporated to treat diffuse scattering in RT [3].

RT is suitable for multiband simulations. If the map or RT model is parametrized with the electromagnetic properties of the constructive materials at different frequencies, the simulations of links operating simultaneously in different bands is straightforward.

RT models are based on 2D or 3D maps of the environment. The level of details in the environment adds complexity to the simulations and accuracy to the results. The complexity of the maps defines the efforts expended during the acquisition of the models. However, nowadays with the available technology on point cloud laser scanners, this effort is minimized compared to a handcrafted map. In addition, unprecedent levels of accuracy and details can be obtained. However, including too many objects and details in the map requires larger computation efforts during the simulation phase. Therefore, a trade-off is always required between the accuracy on the maps and the computation time and power during the simulations.

In this document, we focus on the derivation of a RT model from accurate point cloud data obtained out of 3D laser scans of the environment in a real industrial setting at a BOSCH factory. This RT model can be used as a pure standalone deterministic model, or it can be integrated as the deterministic component in a hybrid stochastic/deterministic model.

A simple workflow of the process described in this document is shown in Figure 1 and the details for each step are addressed in the following sections.

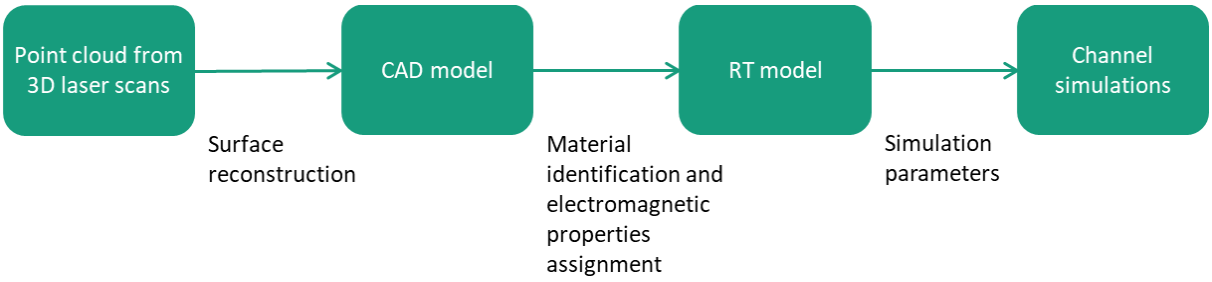

Figure 1 – Workflow from 3D laser scans to RT simulations

1.1 Objective of this document

The main objectives of this document can be summarized as follows:

- Introduce RT as the deterministic propagation modelling tool for simultaneous multiband simulations showing the advantages and disadvantages of this approach for channel modelling in industrial scenarios.
- Describe the scenario on which the RT model was based.

- Introduce the workflow and processing methodology to transform the point cloud data obtained from 3D laser scans in a particular industrial scenario into CAD models for RT applications (Steps 1 to 3 in Figure 1).
- Introduce the resulting RT model and a preliminary comparison with multiband RF measurements at sub-6 GHz and mm-waves conducted in the same premises.
- Define the interface of the model according to the structure of the 6G BRAINS work packages and simulations requirements.

1.2 Relation to other deliverables within the WP3

This deliverable introduces the first component in the chain of steps to obtain a channel model calibrated and verified from measurements. As shown in Figure 2, D3.1 presents the RT model used as channel model in 6G BRAINS. This model is obtained from point cloud data measurements. Later, D3.2 and D3.3 are related to the design of the multi-band measurement equipment and the RF measurement campaigns for RT calibration purposes, respectively. Deliverable D3.4 deals with the calibration and verification of the RT model, based on RF measurements. This step is divided in the calibration and verification of the CAD model by identifying differences between the geometrical properties obtained from the measured propagation paths and the geometry of the scenario, and then the calibration and verification of the electromagnetic properties of the assigned materials to the RT model is performed by comparing the amplitude levels of the different paths identified in the measurements. Finally, once the RT model is verified and calibrated, stochastic components obtained from the measurements are incorporated to the RT results to obtain the fused multi-band channel model for industrial scenarios. Deliverable D3.5 finally addresses the results based on the integration of the waveforms under test into the simulations.

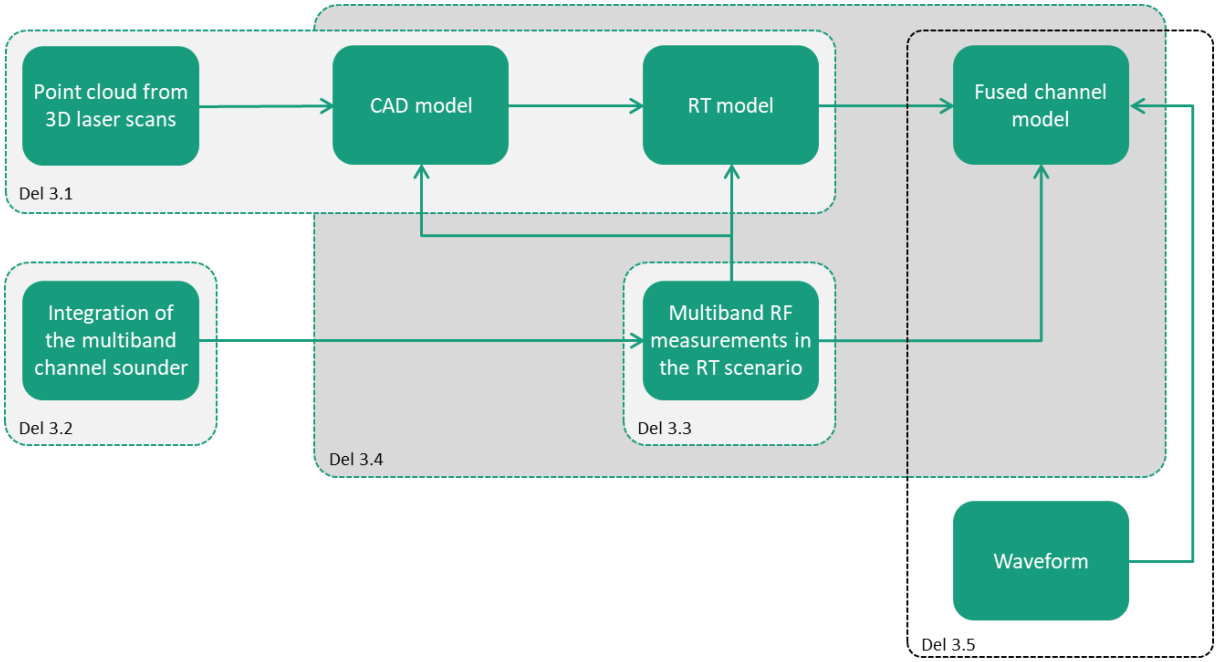

Figure 2 - Relation between workflow and deliverables

1.3 Structure of this document

The rest of the document is organized as follows: in Section 2 we introduce and overview of RT as a channel model for industry scenarios, addressing the pros and cons of such a tool for these applications. In addition, we present the concept of the fused channel model and the interface to other work packages within 6G BRAINS. In Section 3 we develop the workflow and methodology to obtain a RT model from 3D laser scans. Finally, in Section 4 we introduce the results of the different steps shown in the workflow in Figure 1, a preliminary comparison of the RT simulations with multi-band RF measurements conducted in the same scenario, and a comparison of results using different RT tools. A conclusion is finally summarized with future tasks in Section 5.

2 Overview of Ray Tracing as Channel Modelling Tool for Industry Scenarios

Mm-Waves and THz systems rely on the utilization of high directive radio interfaces to compensate the increased isotropical path-loss with frequency. Therefore, the implementation of such a system requires the knowledge of the direction in which the gain (given by a beam-former or a highly directive antenna) of the radio interface must be steered. Hence, DoA and DoD are fundamental parameters for the design, test, and operation phase.

In multipath channels, the DoD and DoA of the LOS component depends only on the position of the APs and UEs. On the other hand, the directions of the transmitted, scattered, diffracted, and reflected paths depends also on the location of the interacting objects in the environment. In addition, if mobility is supported, DoD and DoA changes during the displacement and an update on these parameters is necessary. Therefore, spatial consistency in these models is critical to test these applications.

SCMs based on the 3GPP guidelines [4] offer the possibility to simulate the spatial conditions of the channel. These models provide CIRs based on large-scale parameters (LSPs) obtained from stochastic distributions that are parametrized from measurements. In this stochastic modelling approach, the propagation parameters of the MPCs associated to the geometry of the scenario, i.e., ToF, DoD, and DoA, are obtained from the delay spread (DS), azimuth spreads of departure (ASD), elevation spread of departure (ESD), azimuth spread of arrival (ASA), and elevation spread of arrival (ESA), respectively. These LSPs are generated from stochastic distributions, and therefore, there is no real association between the position of scatterers and the propagation distance, DoD, and DoA of paths. Moreover, in the 3GPP-like models, there is no absolute value of the delay of the NLOS paths, burdening the implementation of methods based on the time of arrival [1]. This results in unrealistic descriptions of the geometry of the environment, limiting the usability of these models for applications in which spatial consistency is required[2], e.g., for beamforming during mobility, and for applications in which a deterministic picture of the geometry of the environment is important, e.g., for integrated sensing and communication (ISAC) and SLAM. Therefore, deterministic models based on RT or ray-launching, in which there is a real correspondence

[1] An extension based on a stochastic approach to provide absolute values to the time of arrival of the multipath components in NLOS is addressed in [26].

[2] Extensions to enable spatial consistency in SCMs based on the 3GPP guidelines can be found in [27].

between the geometrical and electromagnetic properties of the paths and the location of the scatterers, are better suited for the targeted frequencies and applications within 6G BRAINS.

Furthermore, in the latest years there has been an increased interest on multiband applications, i.e., scenarios with multiple devices operating and co-operating at different frequencies, covering from sub-6 GHz to the mm-waves bands. Therefore, there has been a wide number of measurements for a simultaneous characterization of propagation at different frequencies in different scenarios [5], [6], [7], and [8], and multiple activities on standardization of channel models for multiband applications [4], [9]. While stochastic models need the parametrization from measurements in multiple scenarios at different frequencies, RT can provide multiband results by a correct parametrization of the constructive materials at different frequencies, which requires less effort. However, the effort is paid back on the high computation costs during the simulations, and in obtaining a complex model with a rich number of objects and details.

In addition, RT allows the simulation of correlated multiband channels: the location of the scatterers in the scenario is the same for the different bands. Therefore, inter-band algorithms for applications as beamforming or heterogeneous localization and mapping can be tested targeting systems with multiple radio-interfaces.

RT allows a flexible definition of the simulated scenario, in which APs or BSs and UEs can be freely located in the environment. Depending on the RT tool, different features as mobility are supported.

Since RT tools simulate the propagation mechanisms for a site-specific model/map, the result is the deterministic channel corresponding to the map used during the simulations. Hence, the analysis of the results of the applications tested with these models can barely be generalized to other scenarios and conditions.

On the other side, if the model/map contains enough details, the simulations will provide a reliable representation of the propagation in the simulated environment that can be contrasted with real in-situ propagation measurements. Frequently, these measurements are used to adjust, calibrate, and validate the RT model. A validated RT model opens the possibility to sample larger numbers of positions in the simulated map compared to the measurements. Hence, RT allows the collection of a rich data set of channel samples with high resolution in the different dimensions for statistical analysis, which can be further utilized to contribute to pool of data for parametrization of stochastic models such as the 3GPP.

In addition, the deterministic nature of RT accounts only for resolvable paths, e.g., diffracted, scattered, transmitted, and specular paths (SPs), and ignores aspects as dense multipath components (DMCs) [10]. Previous measurements have shown that DMC is not only scenario dependent, but also frequency dependent [5].

Therefore, different kinds of hybrid stochastic/deterministic channel models that combines RT principles with other methodologies are more suitable to cover these scenarios. Multiple examples of such a methodology can be found in the literature: the METIS hybrid model [11], the quasi-deterministic model introduced in [12], a semi-deterministic model based on RT and propagation graph [13], hybrid model based on RT and Vector Parabolic Equation [14], and point cloud based model [15]. Hence, the goal of the multiband channel modelling task within 6G BRAINS is the obtention of a site-specific hybrid model with deterministic components

from RT simulations (using a very accurate map extracted from point cloud data of the scenario) combined with stochastic components obtained from RF measurements.

2.1 Key parameters in RT simulations

The usual parameters that influence the total number of paths, the computation efforts, and the accuracy of the results on RT simulations are summarized in Table 1.

Table 1 - Key parameters of RT tools

Parameter	Description
Interaction types	Propagation mechanisms of the paths that can be transmission, reflection, diffraction, and scattering
Order of interaction	Total number of the different interaction types of a path
Number of rays	Total number of rays per TX-RX link
Dynamic range	Limits the dynamic range of the paths considered in the simulation
Maximum path loss	Limit of the weakest path strength in the simulation
Length of wedges	It influences the calculation of the diffracted paths
Material properties	Influences the calculation of the scattered power
Number of different materials	This defines the capability of the tool to consider different constructive materials of the elements during the simulations

2.2 Channel impulse response from RT simulations

For each TX-RX link, RT tools usually provide the following per-path information:

- τ_l: time of flight,
- ϕ_{A_l}: azimuth of arrival,
- θ_{A_l}: elevation of arrival,
- ϕ_{D_l}: azimuth of departure,
- θ_{D_l}: elevation of departure,
- $\gamma_l^{\phi\phi}$: amplitude in the TX ϕ – RX ϕ polarization,
- $\gamma_l^{\phi\theta}$: amplitude in the TX ϕ – RX θ polarization,
- $\gamma_l^{\theta\phi}$: amplitude in the TX θ – RX ϕ polarization,
- $\gamma_l^{\theta\theta}$: amplitude in the TX θ – RX θ polarization.

The supra index $\mathrm{pol} = \{\phi\phi, \theta\phi, \phi\theta, \theta\theta\}$ of γ_l^{pol} is the TX-RX polarization, where ϕ represents the polarization in the ϕ direction in spherical coordinates (usually associated to the

nomenclature “horizontal”), and θ represents the polarization in the θ direction (usually associated to the nomenclature “vertical”).

The multi-dimensional dual-polarized SISO CIR $\mathbf{H}(\tau, \phi_A, \theta_A, \phi_D, \theta_D)$ can be constructed with these parameters and represented as a matrix:

$$\mathbf{H}(\tau, \phi_A, \theta_A, \phi_D, \theta_D) = \cdots$$
$$\cdots \sum_{l=1}^{L} \alpha_l \underbrace{\begin{bmatrix} \gamma_l^{\phi\phi} & \gamma_l^{\theta\phi} \\ \gamma_l^{\phi\theta} & \gamma_l^{\theta\theta} \end{bmatrix}}_{\mathbf{\Gamma}_l} \delta(\tau - \tau_l)\delta(\phi_A - \phi_{A_l})\delta(\theta_A - \theta_{A_l})\delta(\phi_D - \phi_{D_l})\delta(\theta_D - \theta_{D_l}), \quad (1)$$

where L is the number of MPCs, α_l is the free space path-loss attenuation, and $\mathbf{\Gamma}_l \in \mathbb{C}^{2\times 2}$ is the dual-polarized complex scattering matrix.

In the case of LOS component, the polarimetric scattering matrix $\mathbf{\Gamma}_l$ is defined as the identity matrix

$$\mathbf{\Gamma}_l = \begin{bmatrix} 1 & 0 \\ 0 & 1 \end{bmatrix}. \quad (2)$$

The channel impulse response in Eq. 1 is antenna and bandwidth independent. Antenna patterns and an arbitrary system bandwidth can be integrated in post-processing steps.

2.2.1 Inclusion of antenna patterns in the channel impulse response

The channel impulse response from Eq. 1 considers isotropic antennas. The antenna pattern, single or dual-polarized, can be included by weighting each path with the antenna gain in the direction of the DoD at the TX and the DoA at the RX:

$$h(\tau) = \sum_{l=1}^{L} \underbrace{\mathbf{g}_{\mathrm{RX}}^T(\phi_{A_l}, \theta_{A_l})\mathbf{H}_l(\tau_l, \phi_{A_l}, \theta_{A_l}, \phi_{D_l}, \theta_{D_l})\mathbf{g}_{\mathrm{TX}}(\phi_{D_l}, \theta_{D_l})}_{\gamma_l} \delta(\tau - \tau_l), \quad (3)$$

where $\mathbf{g}_{\mathrm{RX}}$ and $\mathbf{g}_{\mathrm{TX}}$ are the RX and TX single polarized antenna patterns, respectively, described as $\mathbf{g}_{\mathrm{TX}}^T(\phi_D, \theta_D) = [g^{\phi}(\phi_D, \theta_D) \quad g^{\theta}(\phi_D, \theta_D)]$, and γ_l is the resulting path amplitude weighted by the TX and RX antenna patterns.

In case of dual-polarized antennas, the antenna patterns are described by a matrix instead of a vector, as shown for the TX example:

$$\mathbf{G}_{\mathrm{TX}}(\phi_D, \theta_D) = \begin{bmatrix} g^{\phi\phi}(\phi_D, \theta_D) & g^{\phi\theta}(\phi_D, \theta_D) \\ g^{\theta\phi}(\phi_D, \theta_D) & g^{\theta\theta}(\phi_D, \theta_D) \end{bmatrix}. \quad (4)$$

Hence, the CIR also becomes a 2×2 matrix due to the two ports of the TX and RX antennas:

$$\mathbf{H}(\tau) = \sum_{l=1}^{L} \underbrace{\mathbf{G}_{\mathrm{RX}}^T(\phi_{A_l}, \theta_{A_l})\mathbf{H}_l(\tau_l, \phi_{A_l}, \theta_{A_l}, \phi_{D_l}, \theta_{D_l})\mathbf{G}_{\mathrm{TX}}(\phi_{D_l}, \theta_{D_l})}_{\gamma_l} \delta(\tau - \tau_l). \quad (5)$$

2.2.2 Inclusion of bandwidth in the channel impulse response

RT simulations account for infinite resolution in the delay domain obtained by an infinite bandwidth B_{RT}. Hence, ToF of paths are not following a sampling grid: the different MPCs are perfectly isolated in the time domain and there is no small-scale fading. However, once an arbitrary bandwidth B is considered in the system, usually determined by the sampling

frequency, the resolution in the time domain and the sampling grid of the band limited system defines the channel taps by $\Delta\tau = \frac{1}{B}$.

A natural approach to limit the bandwidth of the RT simulations to the desired system bandwidth is by analyzing the response of the channel in the frequency domain. The complex base band representation of the frequency response (FR) of the channel with a finite bandwidth B and K frequency samples separated $\Delta f = \frac{B}{K}$ can be represented as

$$H(k\Delta f) = \sum_{k=-\frac{K}{2}}^{\frac{K}{2}-1} \sum_{l=1}^{L} \gamma_l \, e^{-j2\pi \, k\Delta f \, \tau_l}. \quad (6)$$

Afterwards, the CIR is calculated by the inverse Fourier transform of $h(n\Delta\tau) = \mathrm{IFFT}\{H(k\Delta f)\}$.

An example of a RT simulated CIR with infinite and limited bandwidths are displayed in Figure 3. There is a clear decrease on resolution in the time domain when different finite bandwidths are applied. This also shows the effects of bandwidth on the accuracy on estimation in localization. The detail in Figure 3b shows how multiple MPCs are not resolvable anymore, giving origin to small-scale fading.

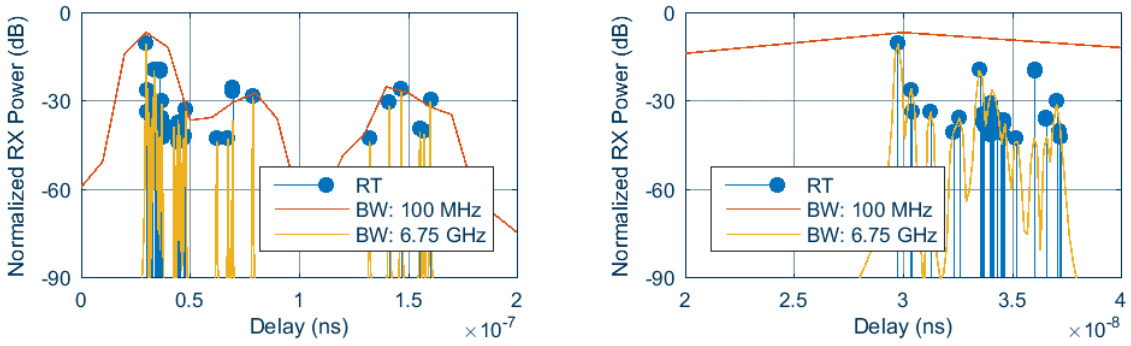

(a) (b)

Figure 3 - Simulated CIR with infinite and limited bandwidth (a) complete, and (b) detail.

2.3 Fused channel model: concept

The global goal of WP3, regarding channel modelling, is to obtain a multiband fused channel model. This model has the different features required to test the applications of interest withing 6G BRAINS:

- Deterministic and realistic localization of scatterers for beamforming, localization, and imaging applications
- Accurate multiband simulations with frequency dependent propagation characteristics
- Realistic propagation properties from RF measurements in industrial scenarios in the frequencies of interest within the 6G BRAINS project.

The model consists of a deterministic component obtained from RT simulations and of optional stochastic components obtained from statistics from multiband measurements and simulations. The fusion is done in MATLAB to obtain a hybrid deterministic/stochastic propagation model. In case that stochastic components are not considered, the model remains purely deterministic. Later, system aspects as antenna patterns and bandwidth can be flexible introduced to obtain the radio-channel model for the different applications under test.

A schematic of the fused channel model is displayed in Figure 4.

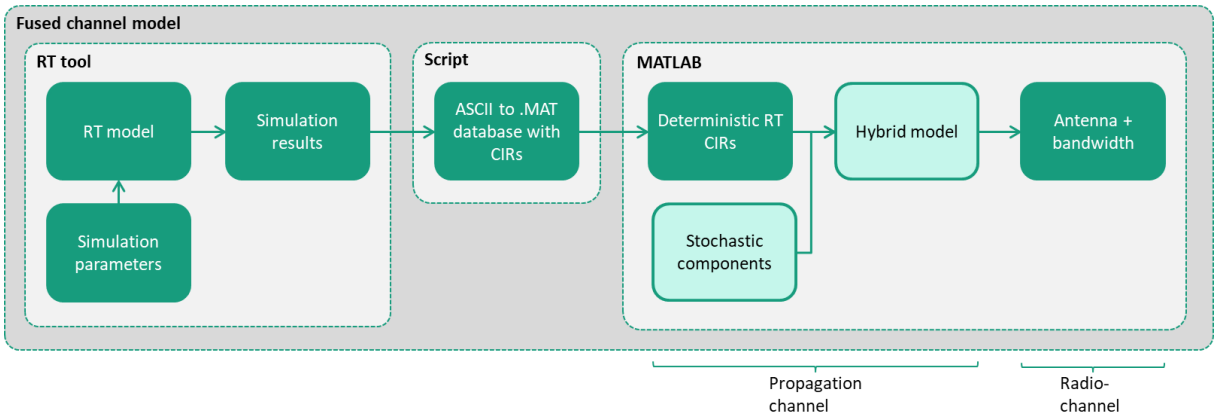

Figure 4 - Concept of the fused channel model

2.4 Applications of Digital Twin

2.4.1 Radio Beam Control

The beam scheduler implements intelligent beam steering that using an antenna array can steer beams from BSs to UE locations efficiently based on interpreted CIR knowledge of uplink isotropic transmissions from uplink UE and then to optimize the beam direction using reinforcement leaning to maximize the SINR and when the path between the transmitter and receiver is broken through an obstruction immediately find and use alternative secondary paths to steer the beam between the transmitter and receiver by avoiding the obstruction. The optimized beam direction from two BSs can also be used to obtain the location of user equipment locations.

The beamforming vector is obtained through DNN by using predicted digital twin isotropic transmissions from user equipment in a grid over the coverage area, and the predicted digital twin measured impulse response at each IAB receiver of 4 polarized transmissions and received power which acts as input information to train a DNN.

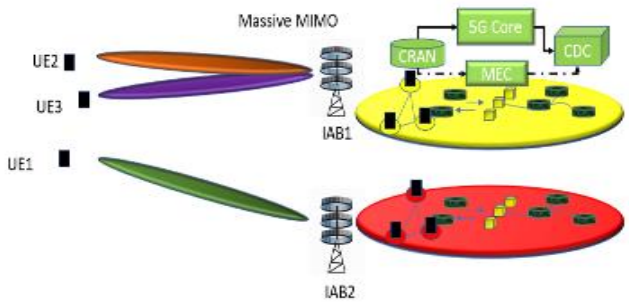

Figure 5 - Radio beam control

The beamform codebook index is the set of beamform vectors comprising of steering angles at the receiver of different alternative secondary paths to steer the beam between the transmitter and receiver by avoiding any obstruction.

In this work, as a result of the absence of a real environment, the beamforming, the power control and interference coordination is jointly carried out on a digital twin to enhance the performance of the 5G network. The proposed network comprises of serving IABs and one interfering IAB. The DRL-NN is modeled for the downlink scenario in which an IAB is serving a UE. The IABs are fixed known distance apart and different UEs are uniformly distributed in a particular service area. Also, the users are moving at a fixed speed. A UE is served by maximum one IAB. Hybrid beamforming for the downlink data transmission is employed to overcome the problem of high propagation loss.

- **State space S:**

$s_t^0, s_t^1 = \mathrm{UE}_1\big(x(t), y(t)\big)$ → Coordinates of UE served by AIB 1

$s_t^2, s_t^3 = \mathrm{UE}_2\big(x(t), y(t)\big)$ → Coordinates of UE served by AIB 2

$s_t^4 = P_{\mathrm{IAB1}}(t)$ → Transmission power IAB 1

$s_t^5 = P_{\mathrm{IAB2}}(t)$ → Transmission power IAB 2

$s_t^6 = \mathbf{b}_{\mathrm{IAB1}}(t)$ → Beamform vector IAB 1

$s_t^7 = \mathbf{b}_{\mathrm{IAB2}}(t)$ → Beamform vector IAB 2

- **Action space A:**

$\mathrm{a}[0] = 1$: Increase the transmit power of IAB 1 by 1 dB

$\mathrm{a}[1] = 0$: Decrease the transmit power of IAB 2 by 1 dB

$\mathrm{a}[1] = 1$: Increase the transmit power of IAB 2 by 1 dB

$\mathrm{a}[2] = 0$: Step down the beamforming code book index of IAB 1

$\mathrm{a}[2] = 1$: Step Up the beamforming code book index of IAB 1

$\mathrm{a}[3] = 0$: Step down the beamforming code book index of IAB 2

$\mathrm{a}[3] = 1$: Step up the beamforming code book index of IAB 2

- **Reward:**

The proposed reward scheme depends on the relevance of the action performed and on meeting the threshold SINR. Agent is rewarded the most in a unit time step based on the power control and beamforming action is taken with respect to the achieved throughput and SINR at the user.

The received SINR, opportunistic throughput for the UE in the particular IAB is monitored based on the changing beamforming vector. The $Q(s,a)$ is updated in every time step and it should converge to the optimal state action value $Q^{+}(s,a_1)$.

To achieve this, a NN with weights is employed as shown in the figure below. The sigmoid function is employed as the output for each hidden node.

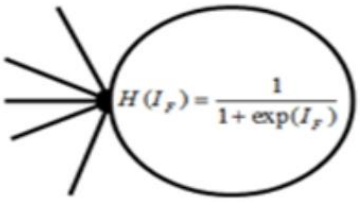

- **The learning algorithm:**

Q learning is a near optimal learning. Therefore, epsilon greedy Q learning is implemented. It has two action modes:

Mode 1- The agent tries different actions at random at every time step t to discover an effective action.

Mode 2- The agent chooses an action at time step t that maximizes the state-action value function $Q(s,a;\theta t)$ based on the previous experience.

- **Training scheme:**

Offline Training would be implemented and post offline training, trained DRL-NN will be implemented in working for real time scenario.

- **Behavior**

Initial simulation is performed on MATLAB 2021a for RT using site viewer and simultaneous channel generation. The output of raytracing is fed for channel generation which in turn produces input for the DNN for training. For RT and channel generation different users' locations for fixed BS positions are considered. Channel parameters varies with respect to varying user locations. Therefore, DNN is trained to different channel parameters which in turn is dependent on user location. The DNN is trained on python module and is trained for efficient beamforming the data towards the user. Post training and during the working phase, system performs beam scanning to obtain the channel parameters based on user locations.

Beamforming weights are adjusted from channel parameters to form the beam pointing towards the current user location. In this way, based on the obtained channel parameters the user locations could be estimated.

2.4.2 RAN Scheduler

The main problem in current methods to adapt radio link that use fixed tables for adaptive modulation and coding (AMC) is the delay that happens when a CQI report is generated and the feedback regarding the channel condition. Also, past research has shown that it is difficult to derive accurate link performance predictors under realistic channel assumptions. To tackle this problem, a Reinforcement Learning-AMC method is being developed where the system dynamically chooses the best modulation and coding scheme (MCS) that promotes the maximum throughput based on previous AMC decisions.

Online learning comprises of adaptively learning the CQI, which produces the greatest throughput given the radio channel conditions through exploration, whilst exploiting the knowledge of the CQI that currently produces the greatest throughput from predefined look-up tables. A CQI which is set too high for given channel conditions runs the risk the occurrence of loss of throughput because of block error due to too high QAM order and too low code rate MCS used. A CQI which is set to low for given channel conditions uses too strong a MCS and too high code rate MCS so that fewer bits are available for data transmission thereby resulting in a lower throughput.

3 Methodology

This section describes the workflow and methodology to derive the RT model from point cloud data out of 3D laser scans. The hardware and software tools utilized during the different steps are summarized in Figure 6. While the workflow shows the complete modelling approach, in this document we only focus on the first three blocks: obtaining the RT model from point cloud data out of 3D laser scans. Detailed simulation results will be provided in D3.4.

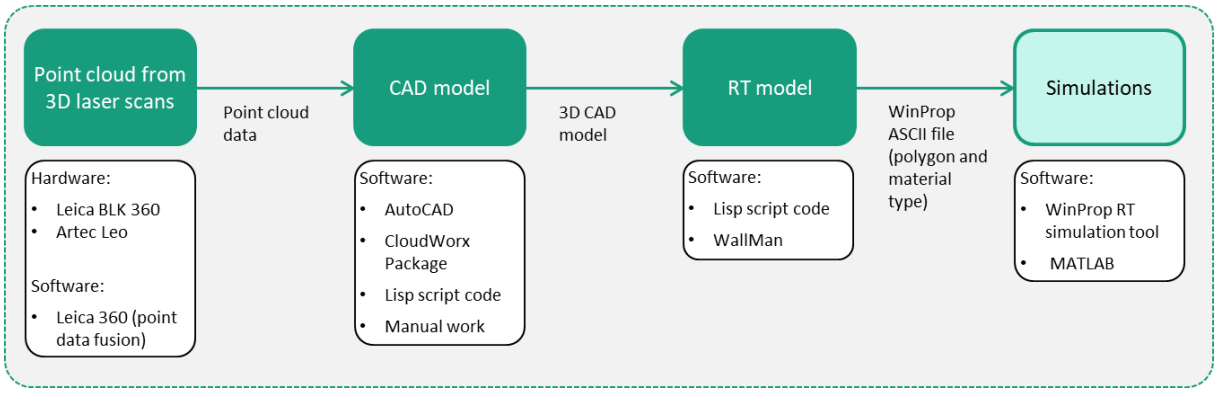

Figure 6 - Hardware and software tools used during the different processing steps

3.1 Point cloud from 3D laser scans

Depending on the dimension of the scenario and objects, the point cloud data was obtained using two different laser scanners, shown in Figure 7. Later, the data of the different scans was combined in a single macro model.

(a) (b)

Figure 7 - Pictures of the laser scanners used during the measurements: (a) Leica BLK360, and (b) Artec Leo.

The laser scanner Leica BLK360 is suitable for small or large range scenarios. At the recommended scanning distance of 10 m, the BLK360 has 6 mm accuracy. Usually, less than 10 scanning positions are necessary in an office scenario to obtain its 3D model. Nevertheless, due to the large size and dense environment of industry scenarios, not only the number of scanning position was increased, but also the scenario is divided into several parts, which are modelled separately with polygons and then combined in a latter step. In this way, the time of generating a single global point cloud data based on all the scans is reduced.

If the different parts of the model are not combined precisely, this step can originate a mismatch on the location of the different objects in the environment. Therefore, the geometrical properties of the model must be validated from RF measurements with high resolution in at least one of the geometrical domains (time or angle).

On the other hand, industrial settings contain multiple machines, such as metallic and curved robot arms, that feature complex structures and high reflective materials. Hand-held scanners are more suitable to characterize these details since they can scan these machines from different angles than the BLK360. However, the advantage of high-resolution leads to large size of the scanned data. Therefore, these kinds of scanners are more suitable only to focus on local objects, usually within the area of 10 m^2.

The industry scenario presented in this document was divided into 4 separate parts, each of approximately 400 m^2, which at last is merged using a common reference column from the scenario. The positions for the macro scans (using the BLK360 scanner) were selected as shown in Figure 8, avoiding blind angles. A trade-off between scanning positions and

resolution resulted in a distance of approximately 1 m between two adjacent scanning positions. Thus, the total number of macro scan positions was at least 100.

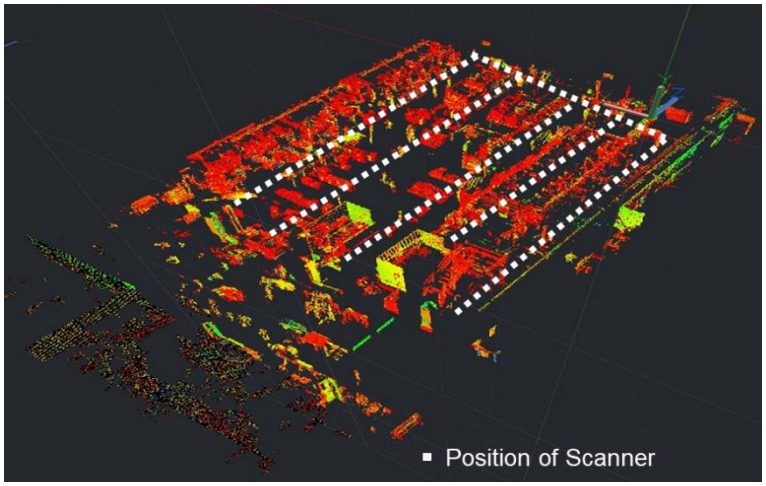

Figure 8 - Positions of the BLK360 laser scanner during the measurements process

On the other hand, the hand-held scanner Artec Leo was used to obtain the point cloud of the machines as shown in Figure 14. Magnetic marks with a particular reference pattern and an index number were added on the metallic frame of each machine, as shown in Figure 9, to correctly place the machines in the macro model of the scenario.

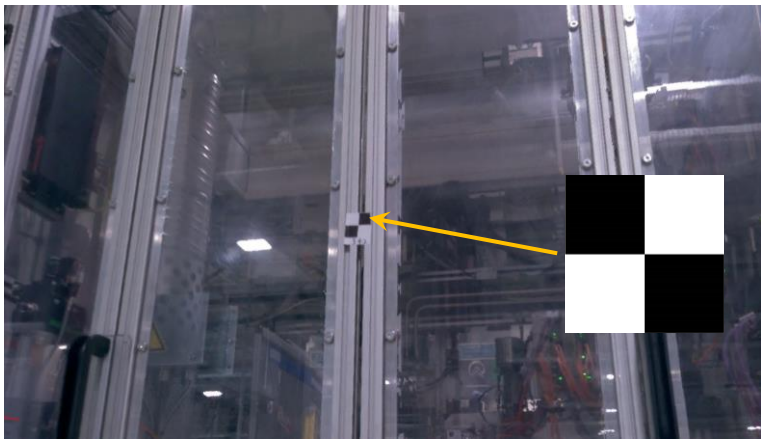

Figure 9 - Magnetic tag with reference pattern for hand-held scanner

3.2 CAD model from point cloud data

The CAD model is obtained by surface reconstruction from the point cloud data. For this reverse-engineering task, we have used commercial tools and CAD software: Leica Cyclone REGISTER, AutoCAD (with package CloudWorx and LISP scripts).

The first step for the generation of the CAD model based on multiple point cloud data is to merge the different scans into a single point cloud file. For this task, we have used the Leica Cyclone REGISTER with help of some common geometry references scanned at different

positions, such as spherical objects, cylinder pipes, and target marks as the ones displayed in Figure 9. The result of this process is a single point cloud file containing the information of the complete scenario.

Then, the merged point cloud data is imported into AutoCAD and the objects are approximated and modeled by simple basic geometric elements/pieces (i.e., cubes, cylinder, and polygons), which can be interpreted by RT tools. To accelerate this task, we have used the CloudWorx package and LISP scripts.

3.3 RT model

The RT model includes not only the geometrical information of the different elements in the environment, but also the constructive material properties of each element. In this scenario, we have classified up to five different materials: metal, concrete, plaster, wood, and glass. The initial material types and properties (permittivity and conductivity) were identified from visual inspection and parametrized following the ITU recommendation [16]. These properties can be later updated from measurements of different material samples [17], or calibrated from RF measurement in the modelled scenario [18] .

Table 2 - Initial electromagnetic properties of materials

Material	Permittivity	Conductivity
Vacuum	1	0
Metal	1	1e+07
Concrete	5.31	0.19305
Plasterboard	2.94	0.054914
Wood	1.99	0.049528
Glass	6.27	0.059075

In 6G BRAINS, we will apply a hybrid methodology to calibrate this RT model with RF measurements. Firstly, the initial electromagnetic properties of the materials are assigned to the corresponding objects, according to the ITU recommendation in [16], as shown in Table 2. Secondly, those properties will be adjusted from RF measurements conducted in the scenario and presented in D3.3, as described in Figure 2. Then, based on the simulated and measured power delay profiles, multiple paths reflected from the same objects/materials can be determined. A system equation based on Fresnel equations and Snell's law is obtained with multiple unknown variables (permittivity and conductivity). If the number of equations is more than two, the problem turns into solving an over-determined non-linear system equation [19] and the solutions are the calibrated permittivity and conductivity. To increase the accuracy of the calibration process, we search for specular reflected paths avoiding the effects of diffuse multipath components. Therefore, low order reflection paths are preferably selected. These results will be provided in the validation phase of this RT model in D3.4.

3.4 Channel simulations

The RT model can be used in different RT tools, e.g., raytrace toolbox in MATLAB [20], WinProp [21], or Remcom [22]. Due to availability and requirements on the results, we have used the WinProp suite from Altair. A comparison of the results obtained with the raytrace toolbox in MATLAB and the WinProp RT are in Section 4.2.

In a first step, the macro properties of the scenario are defined in the RT tool: location of the APs, carrier frequencies, antenna patterns, TX power, location of the RXs, between others. In our case, the antennas are included in a post-processing step to account with a higher flexibility on the system design, and therefore the antennas were set to isotropic during the RT simulations.

Then, settings regarding the calculation of the propagation paths are defined: types of interactions, maximum number of simulated paths, number of different interactions, maximum dynamic range per position, minimum length of wedges considered for diffractions, etc.

The simulation results are stored in an ASCII file and can be imported for post-processing in MATLAB. In this step, aspects as different antenna patterns and bandwidth, or other stochastic channel components as blockage of certain paths, DMC, etc., can be included.

4 Measurements, Analysis, and Results

4.1 RT model from point cloud data

The scenario corresponds to the industry hall in the Bleichach Bosch factory located in Germany. While the dimensions of the complete hall are 171 m x 74 m x 16 m (LxWxH), only a portion of 42 m x 46 m x 11 m (LxWxH) was modelled as shown in Figure 10. This segment contains three production lines and a storage area.

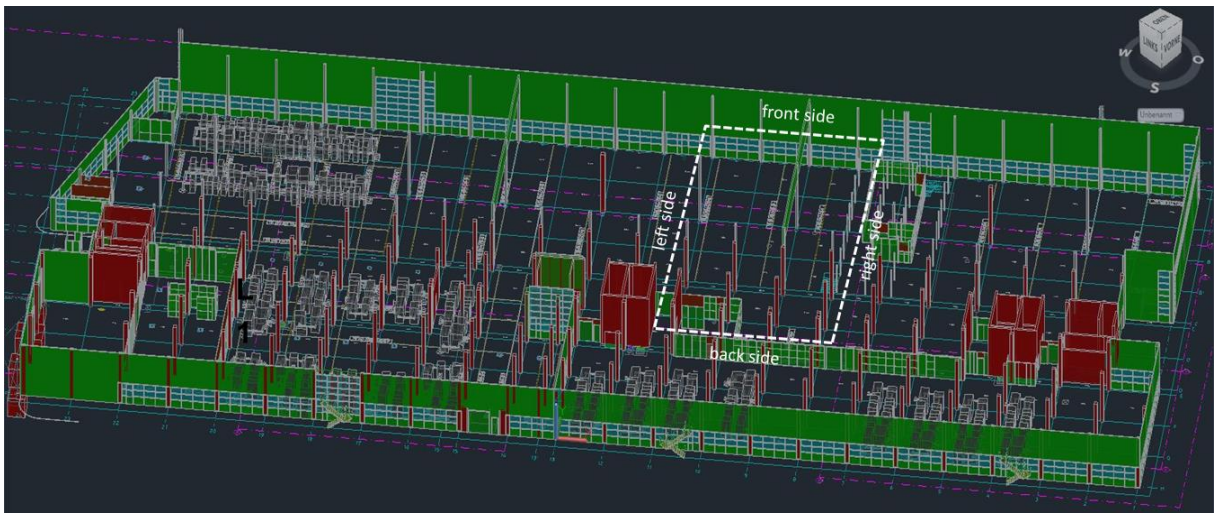

Figure 10 – Modelled portion within the complete map of the factory hall

The limiting walls to the exterior are made from concrete, glass, and metal plates. In addition, concrete columns are mounted in a regular basis along the interior side. Multiple metallic

structures as tubes for ventilation and girders are found close to the ceiling in the upper part of the scenario.

In the measured scenario, 4 different corridors are distinguished between the production lines and labeled as L1, L2, L3, and L4, as shown in Figure 11. These corridors are later used for RF measurements.

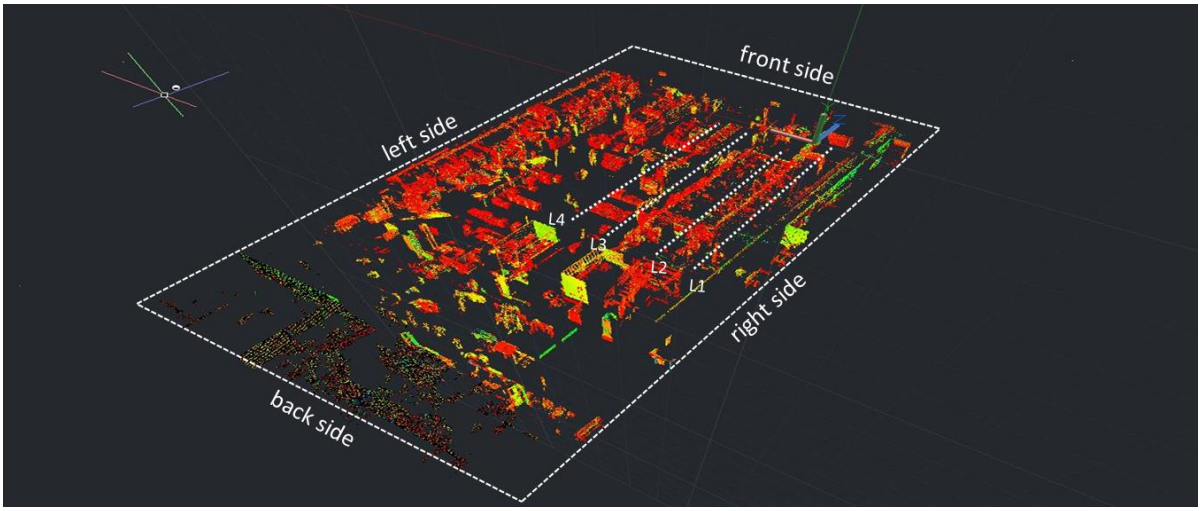

Figure 11 - Point cloud obtained from laser scans in the selected scenario

The point cloud data and CAD model of the complete view of the scenario (without the ceiling for visualization purposes) are presented in Figure 12.

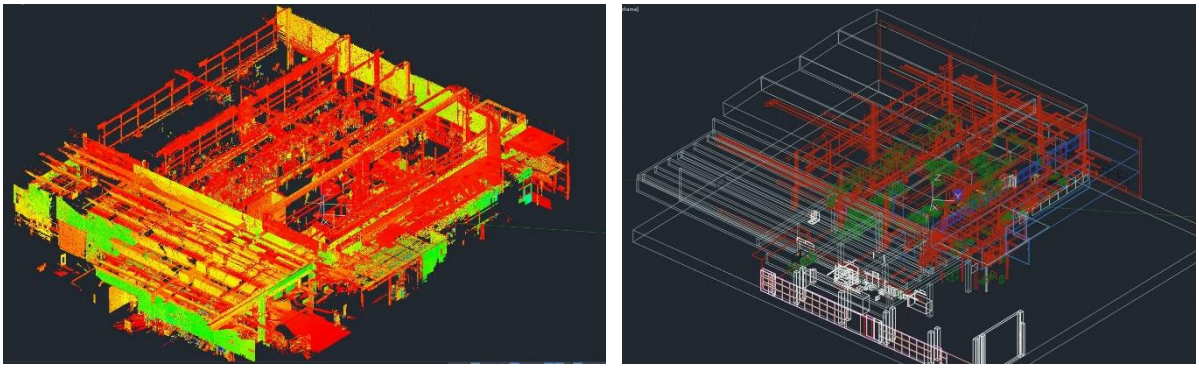

(a) (b)

Figure 12 - (a) Point cloud and (b) CAD model of the measured portion of the scenario (without ceiling for visualization purposes)

Pictures of the borders of the modelled portion of the hall and the CAD model obtained from the point cloud data are displayed to show the level of details in the Figure 13. Multiple objects, especially the ones found in the storage area as mobile cabinets and trolleys have been

included in the RT model during the point cloud scans, but later they were displaced during the RF measurements since the factory was still on operation.

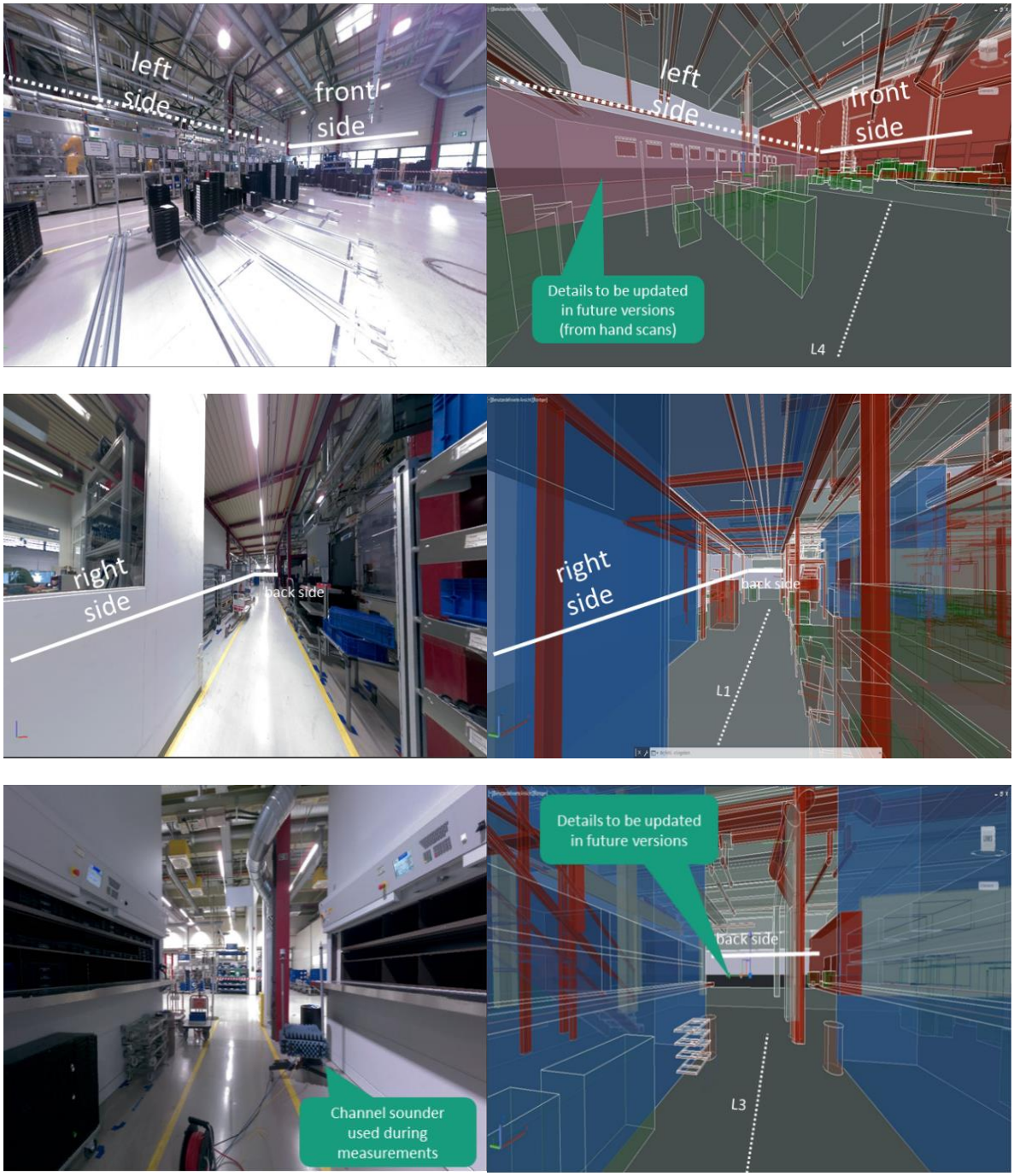

Figure 13 – Pictures and CAD model of the different parts of the scenario

A detail of a machine scanned with the hand-held scanner and its CAD model are displayed in Figure 14, showing the level of details in the model.

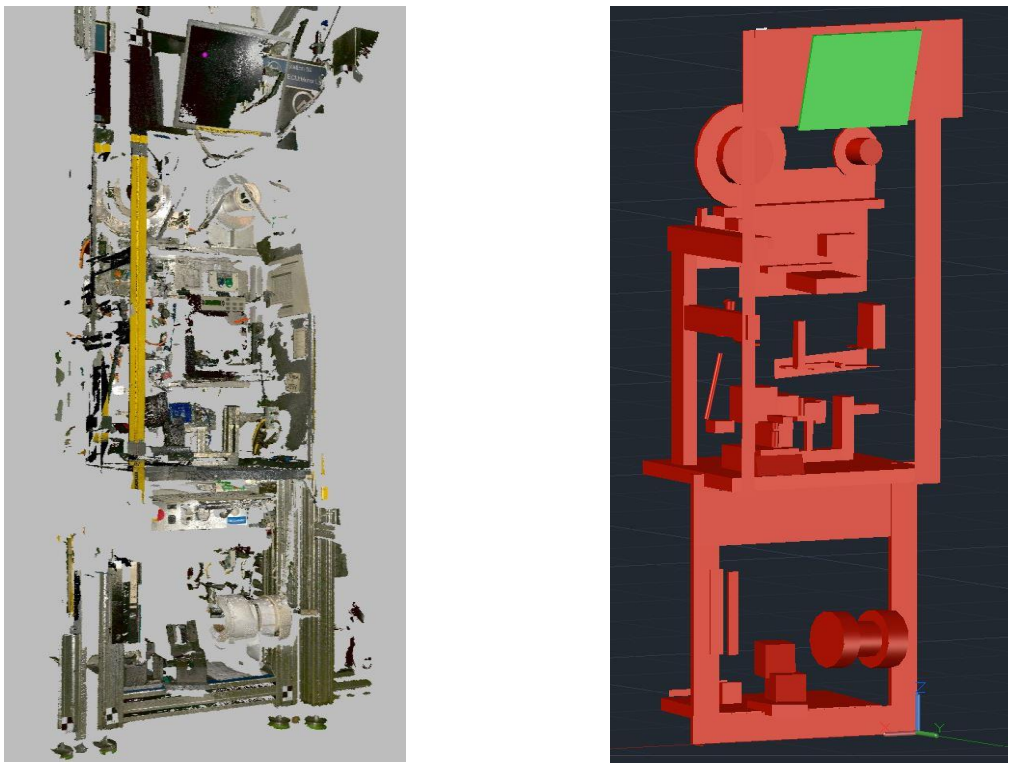

(a) (b)

Figure 14 - (a) Machine scanned with the hand-held scanner, and (b) CAD model

Finally, the CAD and the RT model as it is visualized in WinProp are shown in Figure 15 for comparison purposes.

The resulting RT model after conversion from the CAD model consists of more than 10000 objects. Figures as cubes have been represented with 6 faces, and objects as cylinders (e.g., columns) simplified to 6 rectangular surfaces. It is worth to notice that this influences the interaction type of the rays, since objects as the columns that were originally rounded, in the RT simulations might originate diffracted paths due to the edges of figures into they were simplified or will not generate reflections as a cylinder would do. More objects are expected to be included in future versions of the RT model. Examples are more details on the machines.

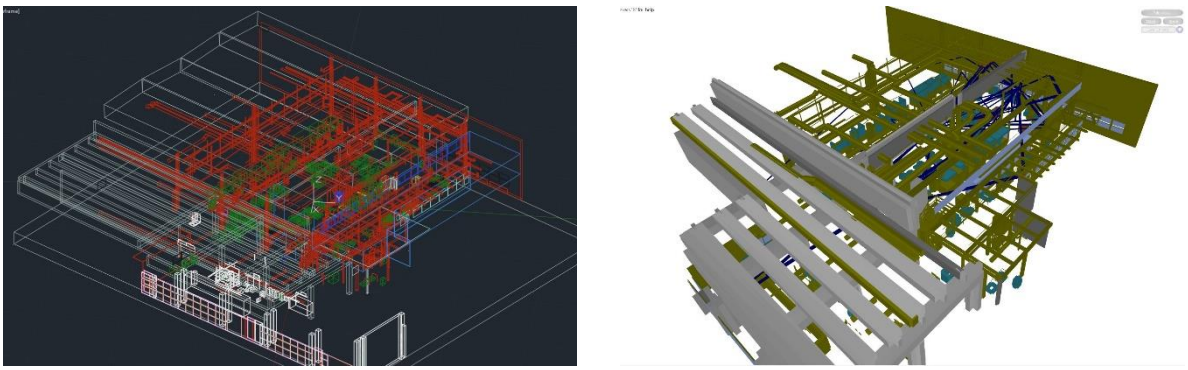

(a) (b)

Figure 15 - (a) CAD model and (b) RT model in Winprop (without ceiling)

In total, 5 different materials have been considered with the electromagnetic properties listed in Table 2. These values will be updated in the calibration phase with the RF measurements in D3.4. The possibility of considering different materials in the simulations allows more realistic results. Otherwise, if a single material is considered during the simulations, the power of the scattered paths only depends on the free-space path-loss.

An example of the visualization of a simulation using this model with the two different ray-tracing tools are displayed in Figure 16.

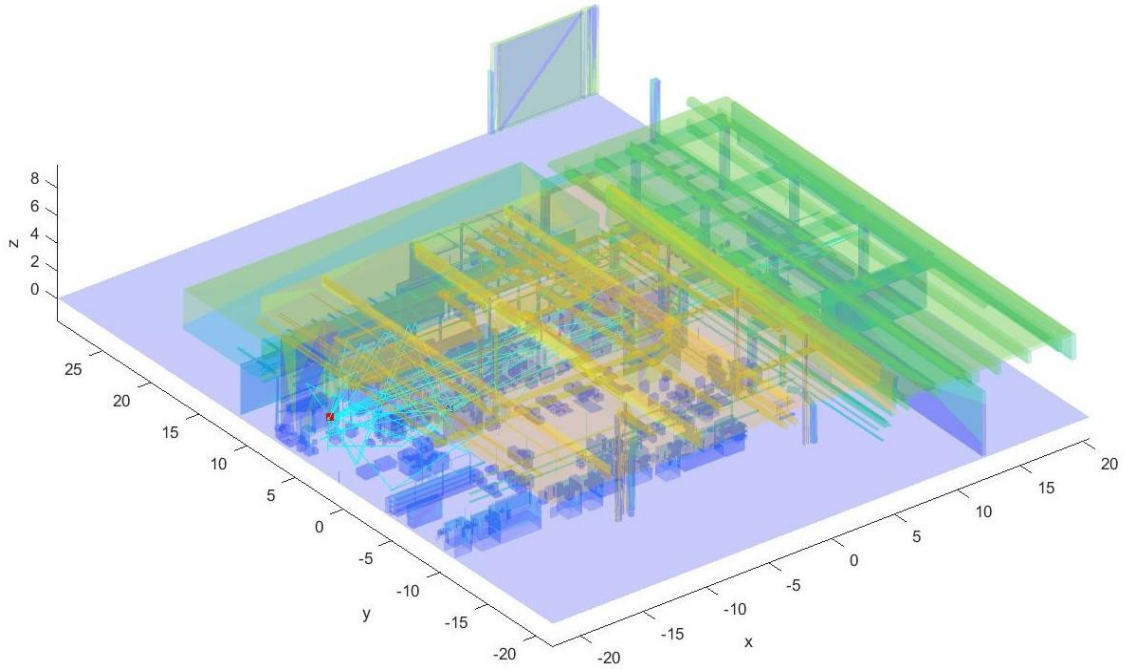

(a)

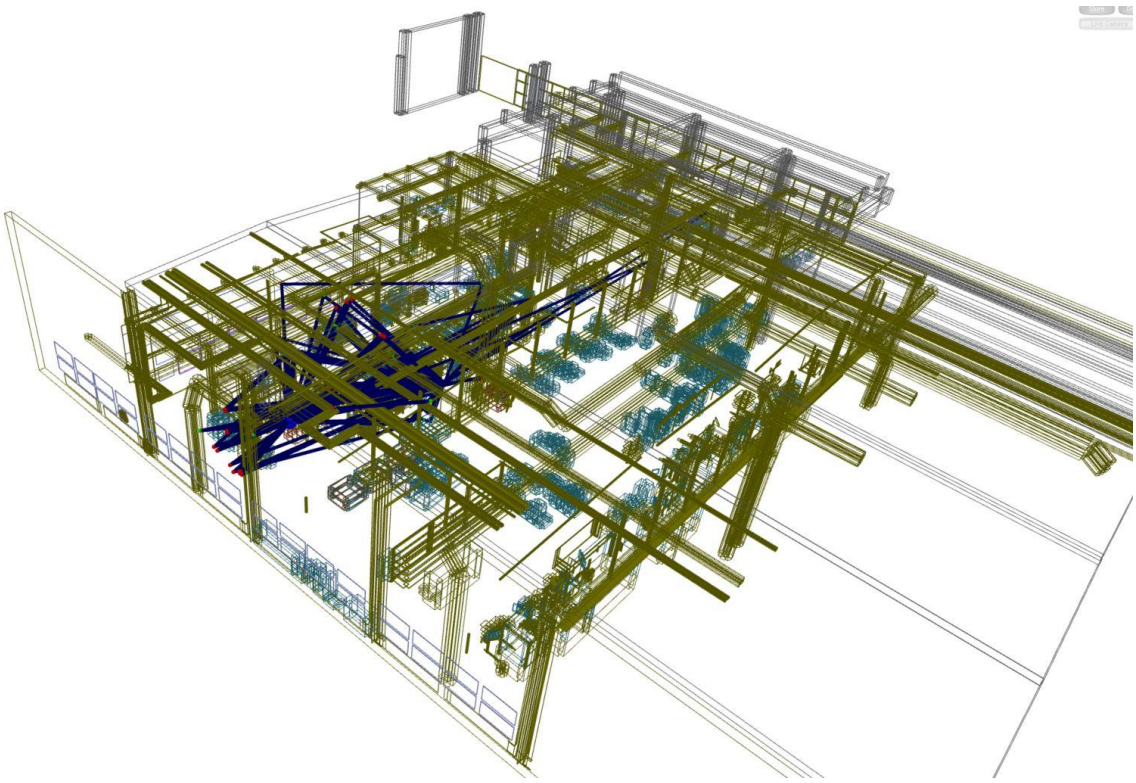

(b)

Figure 16 - Example of the visualization of a simulation with the industry model using (a) MATLAB raytrace toolbox and (b) WinProp

4.2 Evaluation of different RT tools

Once the model/map is obtained from the point cloud data, it can be imported to different RT tools. In this sub-section, we compare the performance of two different RT tools using the same model: the MATLAB raytrace toolbox and the WinProp RT tool.

The MATLAB raytrace toolbox in the current version offers less flexibility on the parametrization of the model: only one constructive material can be selected for all the objects in the scenario. On the other hand, differently to WinProp, it supports round and cylindrical shapes. Moreover, the MATLAB raytrace toolbox doesn't provide the polarization properties of the paths.

A single TX-RX link using the same model has been simulated in WinProp and MATLAB raytrace considering isotropical antennas at 6.75 GHz. Ray-launching has been used in MATLAB

The PDP considering only the first order reflected paths is displayed in Figure 17a. While the time of arrival of the different MPCs is the same in MATLAB raytrace and Winprop, the drawback of considering a single constructive material for all the objects is observed on the power of the different MPCs: the difference of power depends only on the propagation distance (delay). Meanwhile, in the results in WinProp, it depends on the electromagnetic properties of the different materials.

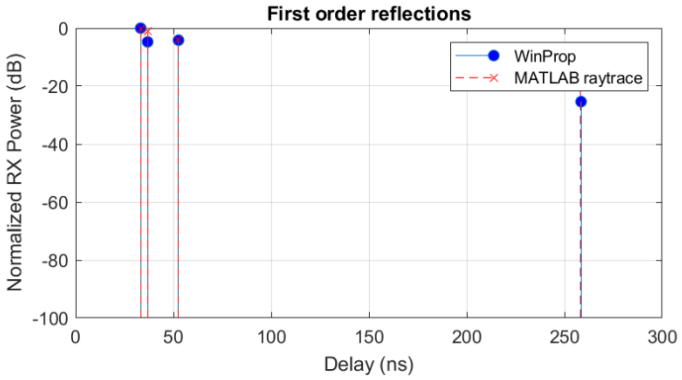

(a)

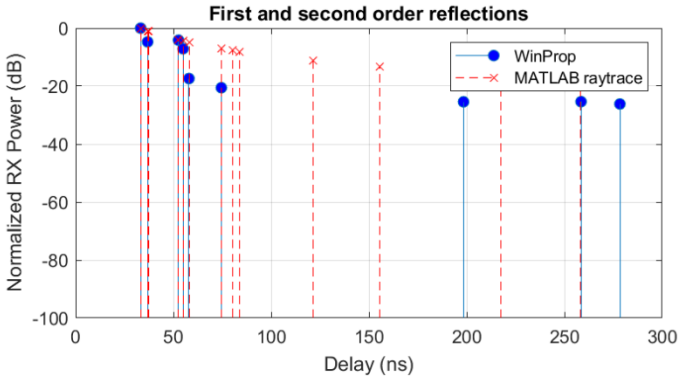

(b)

Figure 17 – Example of a PDP using the same model but different RT tools

In addition, the first and second order reflections are shown in Figure 17b. MATLAB raytrace estimates more paths than WinProp. As shown in Figure 18, most of these paths are from cylindrical objects, since tubes hanging from the ceiling are simplified to 6 rectangular faces in WinProp.

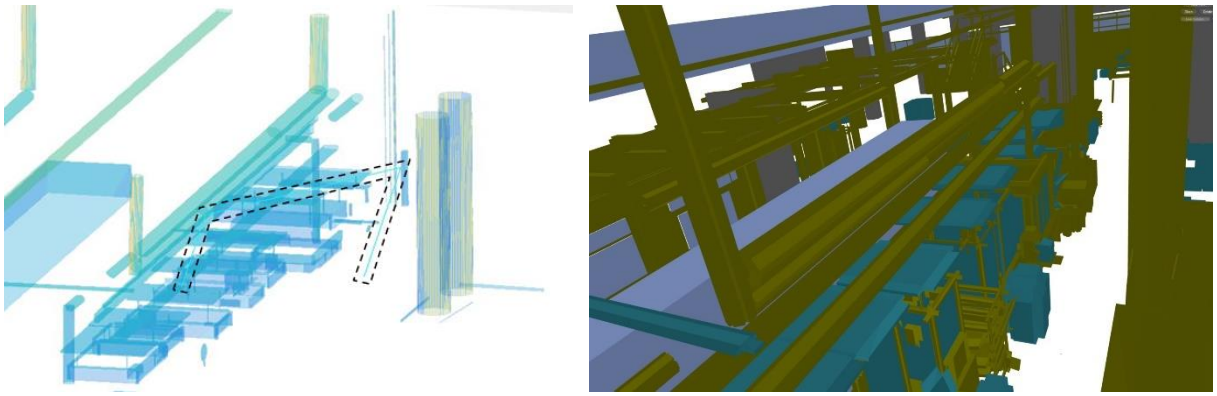

(a) (b)

Figure 18 - (a) Ray visible with MATLAB raytrace tool and (b) not visible in the WinProp tool

Therefore, the accuracy of the results depends not only on the RT model, but also on the features of the RT tool used for the simulations.

4.3 Preliminary RT and RF measurements comparison

Simultaneously, multiband RF measurements at sub-6 GHz, 30 GHz, and 60 GHz bands have been conducted together with the 3D laser scans of the scenario. Therefore, a direct and fair comparison between the RT results and the multiband RF measurements is possible.

A preliminary test on the accuracy on the geometry of the RT model has been done using the propagation distance from the different scatterers (ToF of the paths) as the reference. The objective is to validate the macro structure of the scenario obtained after combining the different CAD models from the point cloud. The methodology is to compare the RT simulation and measured PDPs over the different RX positions in the tracks shown in Figure 19.

4.3.1 Measurement and simulation set-up

The measurements have been conducted with the multi-band ultra-wideband channel sounder developed at the TU Ilmenau [23]. This sounder consists of maximum length binary sequence (MLBS) baseband units with an excitation signal of 15-bits length and a clock frequency (null-to-null bandwidth) of 6.75 GHz.

The baseband units are connected to up and down converters to 6.75 GHz (covering the sub-6 GHz band due to the measurement bandwidth), 33.75 GHz, and 60.75 GHz, labelled as 6.75 GHz, 30 GHz, and 60 GHz for sake of simplicity.

Dual-polarized horn antennas with 30° half-power beamwidth (HPBW) were used to scan the channel at the TX with $\Delta\phi_D = 30°$ steps, from -90° to 90° in azimuth, and from -60° to 30° in elevation, also with $\Delta\theta_D = 30°$ steps. On the other hand, dipoles were used at the RX to save measurement time with the cost of missing the spatial resolution. Therefore, only the vertical polarization was considered for the analysis.

The TX unit was in a fix position at 4.2 m height (above clutter level) at the beginning of track L3. On the other hand, the RX antennas were at 1.36 m height. Multiple points in the scenario were sampled by moving the RX over four different tracks between the production lines, as shown in Figure 11. The sampling RX positions were separated approx. 0.5 m to each other.

A composite picture from the TX towards the different measurement tracks is shown in Figure 19. L1 is NLOS behind two production lines. L2 is also mostly NLOS and is located between two production lines. Finally, L3 and L4 are pure LOS.

Figure 19 - Composite picture taken by the channel sounder at the TX and the different measurement lines (L1 to L4)

The RT simulations were conducted in WinProp with the parameters listed in following table:

Table 3 - RT simulations parameters

Property	Value
Max. transmissions	1
Max. reflections	2
Max. diffractions	1
Max. reflections and diffractions	3
Min. length of wedges considered for diffractions	0.1 m
Max. path-loss of rays	200 dB
Max. number of paths per position	50
Max. dynamic range per position	100 dB

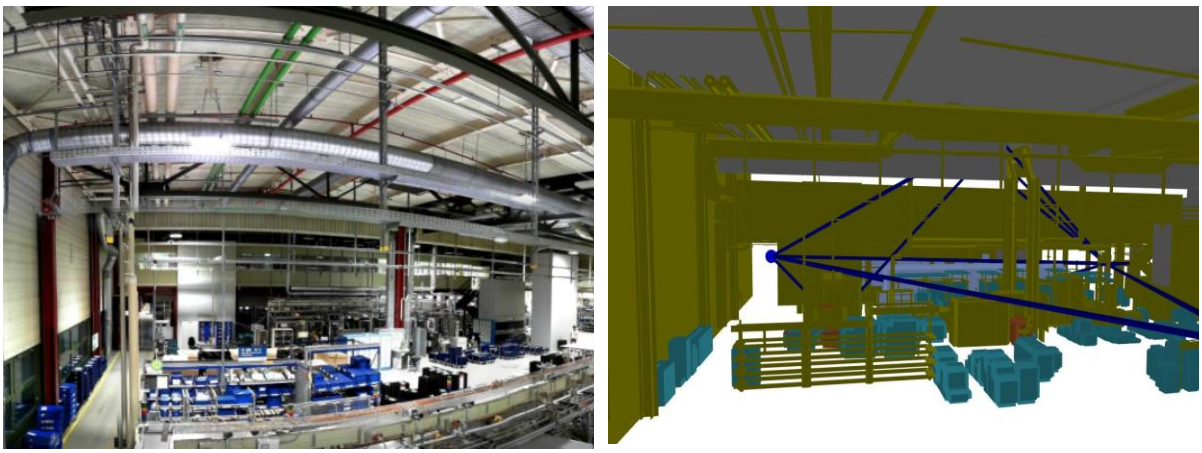

(a) (b)

Figure 20 - Picture of the scenario and RT simulation with the position of the TX used during the RF measurements

4.3.2 Geometry validation from PDPs

Let's define the synthetic omni-directional measured PDP as the average of the PDPs measured over the different angular scans at the TX for each TX-RX measured link:

$$\mathrm{PDP}_{\mathrm{meas}}(\tau) = \frac{1}{I}\frac{1}{J}\sum_{i=1}^{I}\sum_{j=1}^{J}\left|h_{\mathrm{meas}}^{\theta\theta}\left(\tau, i\Delta\phi_D, j\Delta\theta_D\right)\right|^2, \tag{7}$$

where the scanning angles were $\Delta\phi_D = 30°$ with $i = \{-3,-2,-1,0,1,2,3\}$ were $\Delta\theta_D = 30°$ with $j = \{-2,-1,0,1\}$.

On the other hand, since the measurements were not covering the complete sphere in the angular domain, the antenna patterns at the TX (from ideal representations) and the measurement bandwidth $B_{\mathrm{meas}} = 6.75$ GHz were included in a post-processing step in the RT simulations, as described in Section 2.2. Let's consider the RT

$$h_{\mathrm{RT}}^{\theta\theta}(\tau, i\Delta\phi_D, j\Delta\theta_D) = \cdots$$

$$\sum_{l=1}^{L}\underbrace{\mathbf{g}_{\mathrm{RX}}^{T}\left(\phi_{A_l},\theta_{A_l}\right)\mathbf{H}_l\left(\tau_l,\phi_{A_l},\theta_{A_l},\phi_{D_l},\theta_{D_l}\right)\mathbf{g}_{\mathrm{TX}}\left(\phi_{D_l}-i\Delta\phi_D,\theta_{D_l}-j\Delta\theta_D\right)}_{\gamma_l}\,\delta(\tau-\tau_l), \tag{8}$$

where the omni-directional RX antenna was simplified to $\mathbf{g}_{\mathrm{RX}}^{T}(\phi,\theta) = [0\ 1]\ \forall\phi,\theta$, and $\mathbf{g}_{\mathrm{TX}}^{T}(\phi,\theta) = [0\ g(\phi,\theta)]$ is the horn antenna at the TX with $g(\phi,\theta)$ defined from the analytical formula. The emulation of the scanning process in the angular domain is obtained by shifting the antenna patterns to the scanning direction, and evaluating the antenna gain in the direction of the AoD and EoD.

Finally, the synthetic omni-directional PDP of the RT simulations emulating the scanning process was obtained in a similar manner as in (7),

$$\mathrm{PDP}_{\mathrm{RT}}(\tau) = \frac{1}{I}\frac{1}{J}\sum_{i=1}^{I}\sum_{j=1}^{J}\left|h_{\mathrm{RT}}^{\theta\theta}\left(\tau, i\Delta\phi_D, j\Delta\theta_D\right)\right|^2. \quad (9)$$

Therefore, we have three different PDPs to compare: the RT simulated PDPs with isotropic radiators and infinite bandwidth, the RT simulated synthetic omni-directional PDPs from horn antennas with finite bandwidth, and the measured PDPs.

The PDPs in the different RX positions along the track L1 at 60 GHz are shown in Figure 21, showing a good match between the simulated and measured position of the different scatterers.

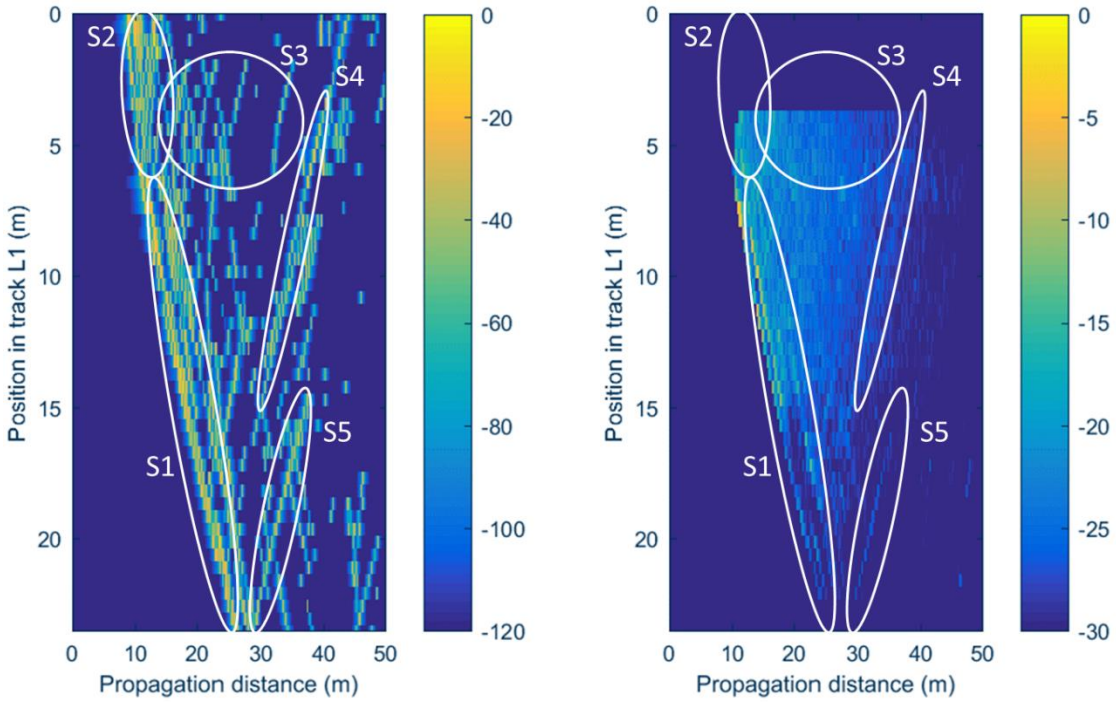

(a) (b)

Figure 21 – Geometrical properties of the scenario from the PDPs at 60 GHz over different positions (a) from RT simulations with finite bandwidth, and (b) from measured PDPs

The different scattering processes indicated in Figure 21 are identified with the help of the visualization tool of the RT in Figure 22. S1 corresponds to a diffracted component on the frames of the machines (indicated as a blue box in the figure) and reflections in tubes hanging on the ceiling. S3 are reflections on the columns located on a regular base. In the measurements only one of these columns are visible at 60 GHz in Figure 21. S4 are paths from the metal stairs, and S5 are paths from a wide column at the end of the track L1.

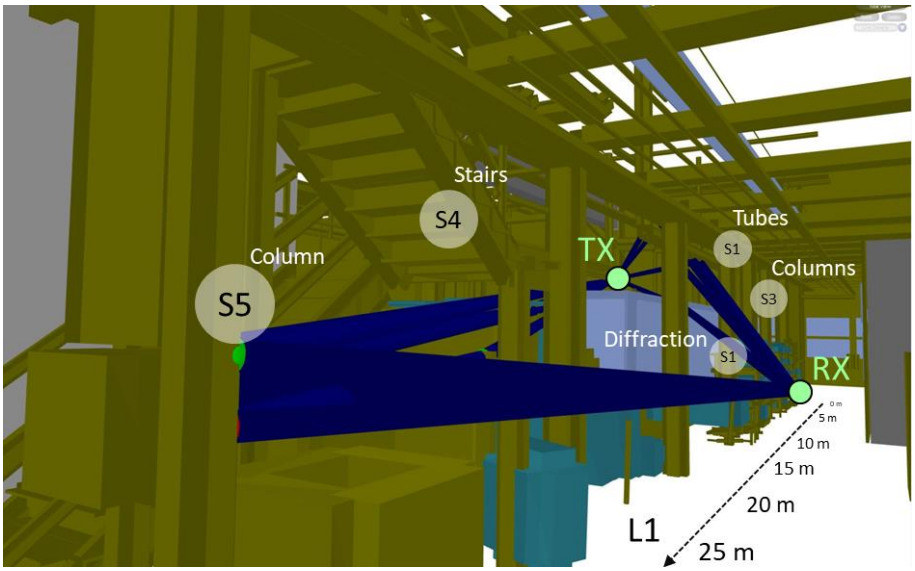

Figure 22 - Interpretation of the scatterers from RT simulations

The missing measured PDPs in Figure 21b (0 m to approximately 3.5 m in track L1) correspond to positions that were discarded due to artifacts or interruptions during the measurements. It is worth to notice that this RT model can accurately predict the PDPs in the missing positions. Therefore, after validation, RT can be used to support measurement campaigns since a higher density on the sampling of the channel can be achieved. In addition, RT facilitates the identification of the different scatterers for a better interpretation of the measurements.

The results have also shown the spatial consistency discussed in Section 2: the dominant scatterers can be tracked during the different positions of the RX.

4.3.3 Geometry validation from PAEPs

Let's define the measured power azimuth/elevation profile as the total received power in the different scanned directions in the angular domain at the TX

$$\mathrm{PAEP}_{\mathrm{meas}}(\phi_D, \theta_D) = \sum_{k=1}^{K} \left| h^{\theta\theta}_{\mathrm{meas}}\left(k\Delta\tau, \phi_D, \theta_D\right) \right|^2, \tag{10}$$

The measured power azimuth/elevation profile for a single position in track L1 and the angular information of the RT simulated paths (in crosses) for the different frequencies are displayed in Figure 23. It can be observed that there is a high density of RT simulated paths in the direction in which most of the power was measured.

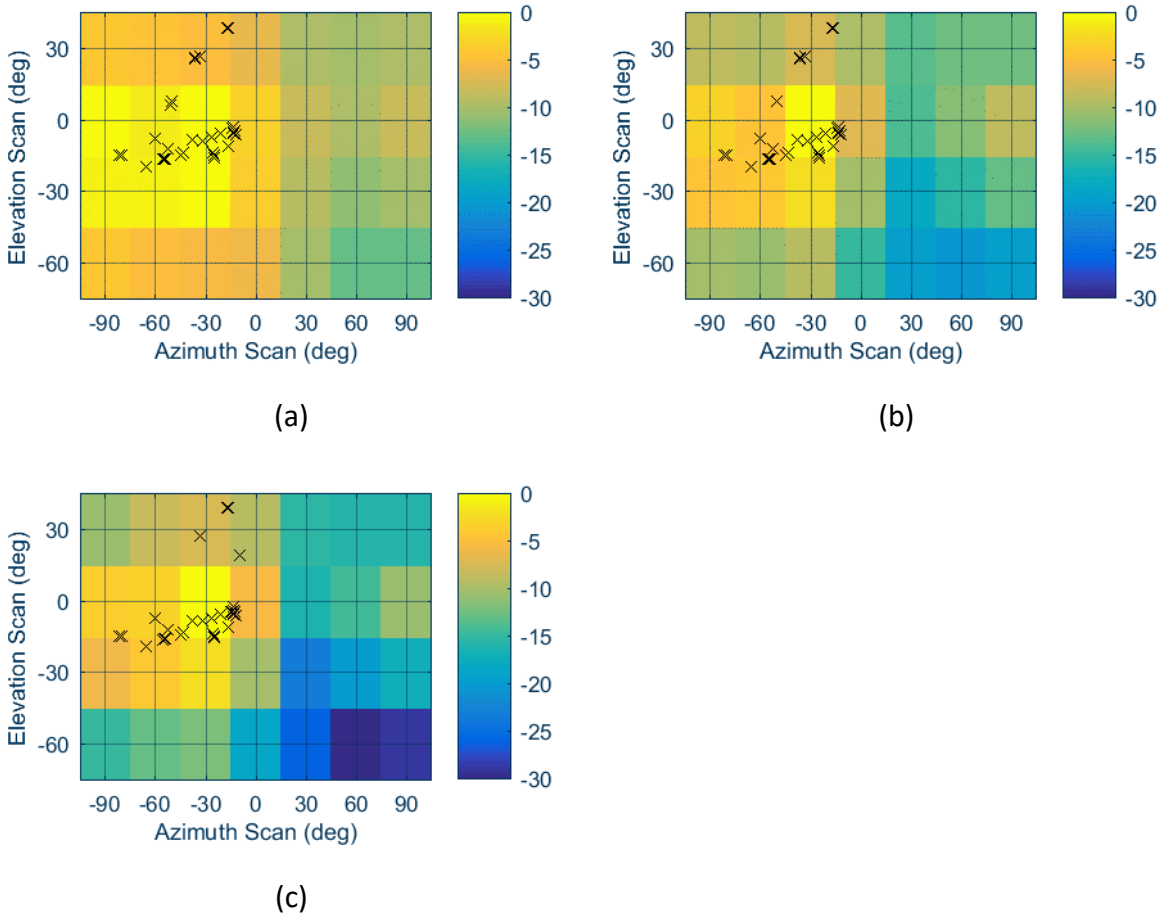

Figure 23 - Measured power azimuth/elevation profile and RT simulation for a single position in track L1 at (a) 6.75 GHz, (b) 30 GHz, and (c) 60 GHz

5 Summary and Concluding Remarks

This deliverable presents the RT model obtained from 3D laser measurements in a real factory. A rich data set of point cloud data has been collected with more than 100 scanning positions within the industrial hall. In addition, a hand-held scanner has been used to obtain higher details of the machines. After the conversion of the point cloud data into CAD models, the different parts have been combined using special marks located in the environment as reference.

RT provides deterministic simulations of the channel with a correspondence between the geometrical characteristics of the environment and the propagation properties of the paths. This allows testing beamforming, localization, and imaging applications, key features within 6G BRAINS. In addition, RT provides spatial consistency over frequency. Therefore, heterogeneous localization methods can be tested with accuracy.

This RT model will be used within 6G BRAINS to obtain a a digital twin of the factory for radio beam control and RAN scheduler.

Since this RT model will be used as the deterministic component in the fused channel model to evaluate the different applications in 6G BRAINS, two different RT tools have been tested

to evaluate the performance. The MATLAB raytrace tool allows to parametrize the different objects with only one material type. Therefore, the difference on the amplitude of the MPCs only depend on the propagation distance (delay). On the other hand, WinProp allows to parametrize the objects with different material types. In our scenario we have selected up to 5 different materials. However, the comparison of the MATALAB raytrace and WinProp tool have shown the absence of some MPCs from reflections in the latter. The reason is the simplification of cylindrical structures in the environment to polygons in WinProp, which originate less specular reflected paths.

The RT model has been compared to multiband RF measurement that were conducted simultaneously during the 3D laser measurements. The preliminary results show a good match between the predicted and the measured MPCs.

In future deliverables, we will conduct a thoroughly validation, and if needed, calibration of the RT by adjusting the electromagnetic properties of the different materials in the environment by comparison to extensive measurements. After the RT model is validated, it can be used to support the interpretation and analysis of RF measurements, and to generate a higher density of channel samples in the environment. The latter is used to obtain statistical aspects of propagation to parametrize stochastic models. In addition, different aspects as human blockage can be further investigated from simulations using this model.

References

[1] R. J. Weiler, M. Peter, W. Keusgen, A. Maltsev, A. P. I. Karls, I. Bolotin, I. Siaud and A. M. Ulmer-Moll, "Quasi-deterministic millimeter-wave channel models in MiWEBA," EURASIP, 2016.

[2] "Deliverable D1.4: METIS Channel Models," 2015.

[3] V. Degli-Esposti, F. Fuschini, E. M. Vitucci and G. Falciasecca, "Measurements and Modelling of Scattering from Buildings," IEEE Transactions on Antennas and Propagation, 2007.

[4] 3GPP , "TR 38.90: Study on channel model for frequencies from 0.5 to 100 GHz," 2020.

[5] D. Dupleich, R. Müller, M. Landmann, J. Luo, G. Del Galdo and R. S. Thomä, "Multi-band Characterization of Propagation in Industry Scenarios," in *14th European Conference on Antennas and Propagation (EuCAP)*, Copenhagen, Denmark, 2020.

[6] D. Dupleich and e. al., "Multi-Band Propagation and Radio Channel Characterization in Street Canyon Scenarios for 5G and Beyond," *IEEE Access,* vol. 7, pp. 160385-160396, 2019.

[7] D. Dupleich and e. al., "Multi-band Indoor Propagation Characterization by Measurements from 6 to 60 GHz," in *13th European Conference on Antennas and Propagation (EuCAP)*, Krakow, Poland, 2019.

[8] M. Boban and e. al., "Multi-Band Vehicle-to-Vehicle Channel Characterization in the Presence of Vehicle Blockage," *IEEE Access,* vol. 7, pp. 9724-9735, 2019.

[9] Mobile and wireless communications Enablers for the Twenty-twenty Information (METIS), "Deliverable D1.4: METIS Channel Models," 2015.

[10] A. Richter, Estimation of radio channel parameters : models and algorithms, Ilmenau: isle, 2005.

[11] I. Carton, W. Fan, P. Kyösti and G. F. Pedersen, "Validation of 5G METIS map-based channel model at mmwave bands in indoor scenarios," in *10th European Conference on Antennas and Propagation (EuCAP)*, Davos, Switzerland, 2016.

[12] A. Maltsev, A. Pudeyev, I. Karls, I. Bolotin, G. Morozov, R. Weiler, M. Peter and W. Keusgen, "Quasi–Deterministic Approach to mmWave Channel Modeling in a Non–Stationary Environment," in *IEEE Globecom Workshops*, 2014.

[13] L. Tian, V. Degli-Esposti, E. M. Vitucci and X. Yin, "Semi-Deterministic Radio Channel Modeling Based on Graph Theory and Ray-Tracing," *IEEE Transactions on Antennas and Propagation,* vol. 46, no. 6, pp. 2475-2486, June, 2016.

[14] X. Zhang, N. Sood, J. K. Siu and C. D. Sarris, "A Hybrid Ray-Tracing/Vector Parabolic Equation Method for Propagation Modeling in Train Communication Channels," *IEEE Transactions on Antennas and Propagation,* vol. 64, no. 5, pp. 1840-1849, May, 2016.

[15] J. Järveläinen and K. Haneda, "Sixty Gigahertz Indoor Radio Wave Propagation Prediction Method Based on Full Scattering Model," *Radio Science,* vol. 49, no. 4, p. 293–305, 2014.

[16] R. I.-R. M.2412, "Guidelines for Evaluation of Radio Interface Technologies for IMT-2020," 2017.

[17] G. D. Chirico, "Device and material characterization at mm-Wave and terahertz," in *Proceedings of the 6th U.K. Europe China Millimeter Waves THz Technologies Workshop (UCMMT)*, Rome, Italy, 2013.

[18] D. He, B. Ai, K. Guan, L. Wang, Z. Zhong and T. Kürner, "The Design and Applications of High-Performance Ray-Tracing Simulation Platform for 5G and Beyond Wireless Communications: A Tutorial," *IEEE Communications Surveys & Tutorials,* vol. 21, no. 1, pp. 10-27, 2019.

[19] L. M. Correia and P. O. Frances, "Estimation of materials characteristics from power measurements at 60 GHz," *5th IEEE International Symposium on Personal, Indoor and Mobile Radio Communications, Wireless Networks - Catching the Mobile Future.,* vol. 2, pp. 510-513, 1994.

[20] MATLAB, 2021. [Online]. Available: https://de.mathworks.com/help/comm/ref/raytrace.html. [Accessed 30 September 2021].

[21] "Altair.com," 2021. [Online]. Available: https://www.altair.de/resource/altair-winprop-datasheet.

[22] "REMCOM," 2021. [Online]. Available: https://www.remcom.com/.

[23] R. Müller, S. Häfner, D. Dupleich, R. Thomä, G. Steinböck, J. Luo, E. Schultz, X. Lu and G. Wang, "Simultaneous multi-band channel sounding at mm-Wave frequencies," in *10th European Conference on Antennas and Propagation (EuCAP)*, Davos, Switzerland, 2016.

[24] "6G BRAINS Consortium," [Online]. Available: https://5g-ppp.eu/6g-brains/.

[25] S. Hur and e. al, "Proposal on Millimeter-Wave Channel Modeling for 5G Cellular System," *IEEE Journal of Selected Topics in Signal Processing,* vol. 10, no. 3, pp. 454-469, April 2016.

[26] D. Dupleich, H. Abbas Mir, C. Schneider, G. Del Galdo and R. Thomä, "On the Modelling of the NLOS First Multi-path Component in Stochastic Spatial Channel Models," in *15th European Conference on Antennas and Propagation (EuCAP)*, 2021.

[27] M. Kurras, S. Dai, S. Jaeckel and L. Thiele, "Evaluation of the Spatial Consistency Feature in the 3GPP Geometry-Based Stochastic Channel Model," in *IEEE Wireless Communications and Networking Conference (WCNC)*, 2019.

[end of document]